PCCP

ROYAL SOCIETY OF CHEMISTRY

PAPER

View Article Online
View Journal | View Issue

Cite this: *Phys. Chem. Chem. Phys.*, 2023, **25**, 29738

Cooperativity between H-bonds and tetrel bonds. Transformation of a noncovalent C···N tetrel bond to a covalent bond†

Xin Wang,[a] Qingzhong Li*[a] and Steve Scheiner *[b]

Received 12th September 2023,
Accepted 19th October 2023

DOI: 10.1039/d3cp04430k

rsc.li/pccp

The dimers and trimers formed by imidazole (IM) and F_2TO (T = C, Si, Ge) are studied by *ab initio* calculations. IM can engage in either a NH···O H-bond with F_2TO or a T···N tetrel bond (TB) with the π-hole above the T atom. The latter is a true noncovalent TB for T = C but is a much shorter and stronger covalent bond with F_2SiO or F_2GeO. When a second IM is added, the cooperativity emerging from its H-bond with the first IM makes it a stronger nucleophile, leading to two minima with F_2CO. The first structure contains a long noncovalent C···O TB and there is a much shorter covalent bond in the other, with a small energy barrier separating them. The same sort of double minimum occurs when the two IM units are situated parallel to one another in a stacked geometry.

1. Introduction

In recent years, there has been a renewed interest in the interactions between molecules that are considerably weaker than the covalent bonds comprising the molecules themselves. These noncovalent bonds play important roles in a myriad of chemical structures and processes.[1–9] In addition to the widely recognized hydrogen bond,[10–12] there is a quickly growing understanding of the halogen bond[13,14] where the bridging proton is replaced by any of Cl, Br, or I. More recent studies have begun to focus on the closely related pnicogen bond,[15,16] tetrel bond,[17–23] and some of their cousins.

In particular, the tetrel bond (TB) has been attracting a good deal of attention in recent years. The TB is a noncovalent bond formed between a group 14 atom on a Lewis acid molecule and an electron donor on a Lewis base.[24] One of the main factors contributing to this interaction is the positive electrostatic potential (σ or π-hole) on the surface of the group 14 atom which attracts a negative site of the nucleophile.[25] Grabowski found that the change in electron charge redistribution caused by the formation of a TB is similar to that in S_N2 reactions, concluding that the formation of a tetrel bond is a preliminary step in S_N2 reactions,[26] amplifying on earlier ideas by Mani and Arunan who replaced one H atom in CH_4 with –OH, –F and –Cl to form tetrel bonds with H_2O, NH_3 and other bases.[27] TBs play a significant role in hydrophobic action and the stability of S_N2 reaction intermediates.[27]

In general, the TB formed by C is quite weak, seldom exceeding 10 kJ mol^{-1}. Nevertheless, this carbon bond is extremely important in the fields of organic chemistry and biochemistry. Such a bond formed by a methyl group with aspartic acid residues helps to inhibit binding with active sites.[28] Biswal and coworkers identified carbon bonds that were common in proteins and accurately measured their interaction energy.[29] This interaction is strong enough to be deemed a significant noncovalent bond that could bind 6MA at the active center of the protein.[29] Carbon bonds present in proteins play an important role in the myoglobin photodissociation mechanisms and the binding of nuclear bases to proteins.[29] Analogous to the σ-hole, a π-hole of positive electrostatic potential occurs directly above a tetrel atom when in a planar molecule. And like the σ-hole, a π-hole can also attract a Lewis base. Hou *et al.* studied the π-hole TBs formed by X_2TO (X = H, F, Cl, Br, CH_3; T = C, Si, Ge, Sn) and CO_2 and found that the interaction energy can be as high as 51 kJ mol^{-1}.[30] Chandra *et al.* identified a C···N π-hole TB between CO_2 and NH_3 by means of infrared spectroscopy and quantum chemical methods.[31]

Cooperativity is a common and important feature of noncovalent bonds. This phenomenon has been recognized for many years in the context of H-bonds, as for example in the process of aqueous solvation. It arises when the charge transfer from one molecule to the other enhances the ability of both to participate in another bond of this sort. Theoretical calculations found that the interaction within the trimer is stronger

[a] *The Laboratory of Theoretical and Computational Chemistry, School of Chemistry and Chemical Engineering, Yantai University, Yantai 264005, P. R. China. E-mail: lqz@ytu.edu.cn*
[b] *Department of Chemistry and Biochemistry, Utah State University, Logan, UT 84322-0300, USA. E-mail: steve.scheiner@usu.edu*

† Electronic supplementary information (ESI) available. See DOI: https://doi.org/10.1039/d3cp04430k

than that in the dimer under the influence of the HB on the tetrel bond.[32] It is worth mentioning that cooperativity is not always reinforcing, but a different alignment of the units can lead to negative cooperativity that weakens the bonds.

In an effort to probe the outer limits of the strength of TBs involving carbon, the F_2CO molecule is considered here in which there exists a healthy π-hole above the C atom. Imidazole (IM) is considered firstly because it is a fairly strong N-base. Secondly and importantly, the other N atom of IM is covalently attached to a H, which can itself serve as proton donor in a HB to a third molecule. The positive cooperativity expected from the first IM acting as both electron acceptor and donor ought to strengthen the TB to F_2CO. The findings for F_2CO are compared to other F_2TO molecules where T represents the heavier tetrel atoms Si and Ge.

High-level *ab initio* calculations are applied to answer several outstanding questions. As the lightest tetrel atom, is C unique or does it share most of its properties with other Group 14 atoms? How strong are the effects of cooperativity on the T···N tetrel bonds, and how might they modify the strength and structure of these complexes? How are these findings altered if the two IM units interact with one another *via* a stacked pair π···π geometry? But also, as described below, the calculations offer a glimpse into a unique and unexpected phenomenon. Without benefit of cooperativity, the C···N interaction is a classic noncovalent bond, with the C···N distance only slightly shorter than the sum of atomic vdW radii. The Si and Ge analogues, however, forgo such a long interaction, with a much shorter covalent T–N bond. However, the cooperativity that occurs when a second IM is added provides a second option for C. Not only is this tetrel bond present in one minimum, but if the two units approach more closely, after overcoming a small energy barrier, they settle into a much shorter bond, with most of the characteristics of a covalent C–N bond within a tetrahedral structure. The cooperativity necessary to induce this highly unusual double minimum character, does not necessarily require a HB between the two IMs, but even a stacked parallel interaction between them is sufficient.

2. Calculation methods

Ab initio calculations were carried out at the Møller–Plesset second-order perturbation theory (MP2) level within the context of the aug-cc-pVTZ basis set since this method has been utilized to study various tetrel-bonded complexes due to its accuracy.[33,34] The geometries of all systems were fully optimized with the aid of the Gaussian 09 set of codes.[35] Harmonic frequency calculations performed at the same level confirmed that these structures are energy minima with no imaginary frequencies. The interaction energy E_{int} is defined as the difference between the energy of the complex and the sum of the energies of the monomers, whose geometries are taken from the complex. The binding energy E_b arises if the fully optimized monomer geometries are used as a reference point. The full counterpoise procedure was employed to correct for the basis set superposition error (BSSE)[36] in both E_{int} and E_b.

The AIM2000 program was used for QTAIM topology analysis of the density,[37] which led to the identification of bond critical points (BCPs) along with associated distinguishing features. Together, Multiwfn[38] and VMD programs[39] yielded NCI diagrams[40] to help visualize the weak interactions. Natural population analysis (NPA)[41] diagonalized part of the density matrix to quantify charge transfer *via* NBO 3.0 version contained in the Gaussian 09 program. Natural orbitals for chemical valence (NOCV) were used to assess the role of molecular orbitals in complex formation.[42] GAMESS software[43] was used for energy decomposition (EDA)[44] of the total interaction energy into physically meaningful components.

3. Results

3.1. Monomers

In terms of their interacting with one another, probably the most important aspect of each monomer is the molecular electrostatic potential (MEP) that surrounds it. The MEP diagrams of the relevant molecules are presented in Fig. 1, wherein red and blue colors refer respectively to positive and negative signs. Both F_2CO and F_2SiO possess a pair of positive π-holes

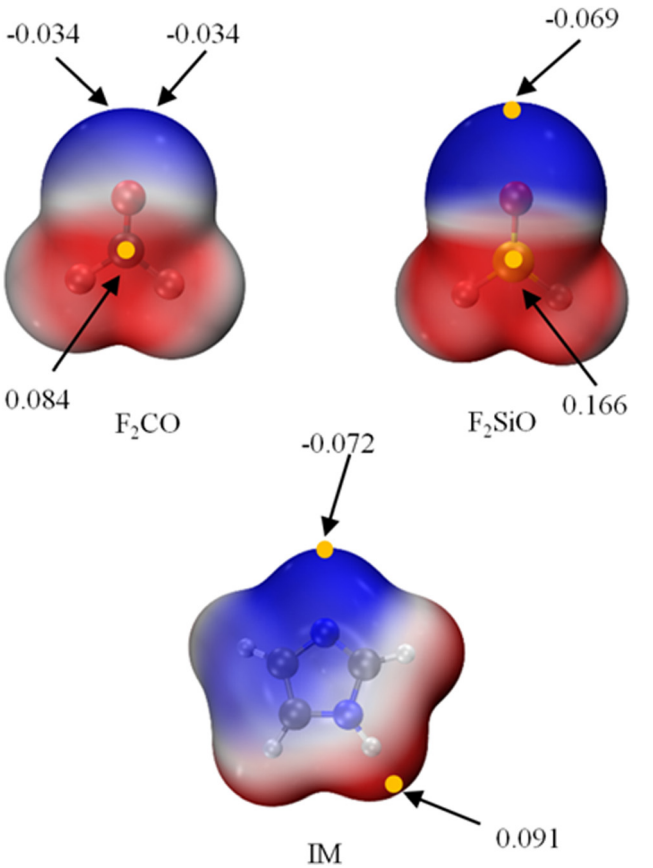

Fig. 1 Molecular electrostatic potential (MEP) maps of F_2TO (T = C, Si) and IM. Red shows the most positive MEPs, while blue shows the most negative MEPs. All in a.u.

above and below the T atom. The hole above F_2SiO is twice as deep as that above F_2CO, with a MEP of 0.166 a.u. as compared to 0.084 a.u. above the C. This is due to the fact that the electronegativity of C atom is larger than that of Si atom. This distinction is consistent with previous studies where the lower electronegativity of the T atom leads to a more positive π-hole.[45] F_2CO has two minima with negative electrostatic potentials on its O atom, while the single minimum in F_2SiO lies directly along the Si=O axis, and is twice as negative as those on F_2CO. These MEP minima are consistent with the O natural charge which is −0.50 e in F_2CO and −1.13 e for F_2SiO. With respect to imidazole (IM), its blue negative MEP coincides with the N lone pair, while the NH group is associated with its most positive MEP.

3.2. Dyads

A pair of IM molecules engage in two sorts of homodimers. The more stable of the two involves a standard NH···N HB, and is labeled 2IM-HB in Fig. 2a. This HB is rather a strong one, with an interaction energy of 43.3 kJ mol^{-1} as listed in the first row of Table 1. The diagram of Fig. 2a shows also that the planes of the two molecules are perpendicular to each other. A perhaps more interesting complex is of a stacked sort, where the planes of the two molecules are parallel to one another. The arrangement within 2IM-π is such that the C–N bonds align with one another in an antiparallel fashion, with two R(C···N) distances of 3.042 Å. The second row of Table 1 shows that this dimer is only slightly less stable than the HB complex, with an interaction energy of 34.6 kJ mol^{-1}. An AIM molecular diagram of this stacked dimer in Fig. 3 confirms that there are two C···N bond paths with a bond critical point density of 0.010 a.u. This quantity is only a fraction of the HB ρ_{BCP} of 0.035 a.u. of the more stable complex, as listed in Table 2. Examination of the individual energy components of these two structures in the first two rows of Table 3 indicates that what the stacked dimer lacks in electrostatic or polarization stabilization, it makes up for in a large dispersion contribution of 37 kJ mol^{-1}. Indeed, the dispersed nature of this sort of slipped parallel arrangement is buttressed by the extensive green weak bonding interaction in the NCI diagram of this complex in Fig. S1 (ESI†).

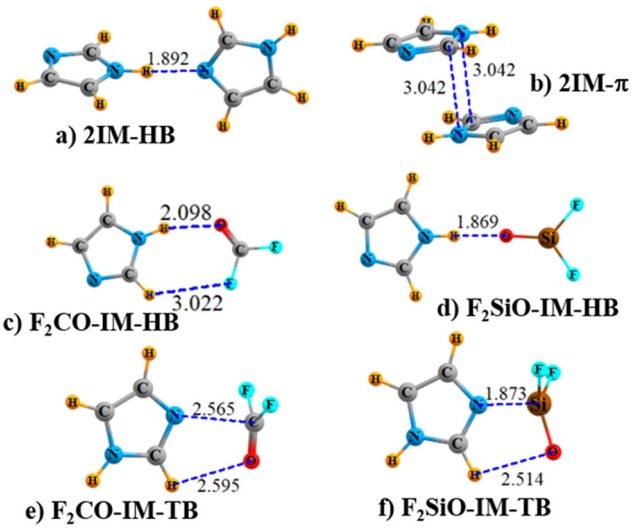

Fig. 2 Optimized geometries of binary complexes with distances in Å.

Table 1 Interaction energy (E_{int}, kJ mol^{-1}), binding energy (E_b, kJ mol^{-1}), charge transfer (CT, e), and NOCV orbital energy (E, kJ mol^{-1}) in the binary complexes

	E_{int}	E_b	CT	E
2IM-HB	−43.30	−41.79	0.030	−27.38
2IM-π	−34.64	−33.10	0	−5.02
F_2CO-IM-HB	−13.93	−13.26	0.006	−4.89
F_2SiO-IM-HB	−29.79	−29.11	0.018	−18.10
F_2CO-IM-TB	−29.87	−27.55	0.013	−13.92
F_2SiO-IM-TB	−258.74	−209.74	0.204	−332.02

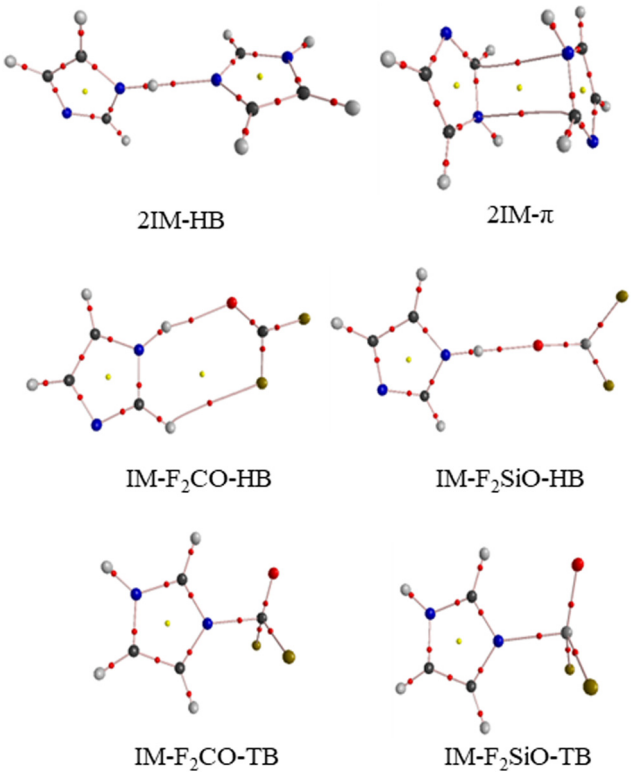

Fig. 3 AIM analysis of binary complexes. Yellow and red dots indicate the locations of ring and bond critical points, respectively.

Table 2 Electron density (ρ), Laplacian ($\nabla^2\rho$), and total energy density (H) at the intermolecular BCP in the dyads, all in a.u

	ρ	$\nabla^2\rho$	H
2IM-HB	0.035	0.077	−0.005
2IM-π	0.010	0.035	0.001
F_2CO-IM-HB	0.002	0.010	0.001
F_2SiO-IM-HB	0.028	0.098	−0.001
F_2CO-IM-TB	0.021	0.065	0.0003
F_2SiO-IM-TB	0.091	0.401	−0.036

Table 3 Electrostatic (E^{es}), exchange (E^{ex}), repulsion (E^{rep}), and polarization (E^{pol}), dispersion energies (E^{disp}) in the binary complexes, all in kJ mol^{-1}

	E^{es}	E^{ex}	E^{rep}	E^{pol}	E^{disp}
2IM-HB	−65.06	−74.64	136.36	−25.44	−14.56
2IM-π	−40.88	−78.28	131.00	−9.54	−36.94
F_2CO-IM-HB	−18.74	−21.46	38.91	−5.52	−7.11
F_2SiO-IM-HB	−45.27	−42.89	78.24	−15.52	−4.35
F_2CO-IM-TB	−62.68	−74.01	135.52	−16.48	−12.18
F_2SiO-IM-TB	−487.27	−466.73	982.07	−323.71	33.05

IM can of course also form a mixed dimer with each of the F_2TO molecules. Structures highlighted by a NH···O HB are exhibited in Fig. 2c and d for C and Si, respectively. The HB is considerably shorter in F_2SiO-IM-HB than in its C analogue, and also the NH···O═Si set of atoms are aligned very nearly in a line. This different angular feature can be understood in part on the basis of the MEPs of the two molecules, in that V_{min} lies directly along the Si═O axis in Fig. 1b, while the two MEP minima in F_2CO diverge from the C═O bond axis. The orientations within the F_2CO-IM-HB complex also permit the formation of a fairly weak CH···F HB, supported by the bond path in Fig. 3. Table 1 shows that the interaction energy for the latter shorter HB is more than twice that for the C analogue, 29.8 vs 13.9 kJ mol^{-1}. The densities of the H···O bond critical point reflect this same pattern, as does its Laplacian. The various contributions to the total energy in Table 3, with $E^{es} > E^{pol} > E^{disp}$, are consistent with its characterization as a HB.[46]

The alternative arrangement for the heterodimers in Fig. 2e and f can best be described as a tetrel bond (TB), with the imidazole N lone pair transferring charge to the π-hole above the T atom, confirmed by the AIM diagrams in Fig. 3. The related N···T distance is much shorter for Si in Fig. 2f, and the result is an enormous interaction energy of 260 kJ mol^{-1}, vs only 30 kJ mol^{-1} for the N···C bond in Fig. 2e. The N···Si critical point density is 0.091 a.u., roughly what may be thought of as a covalent bond, which is echoed by the fairly large negative value of H in Table 2. The partially covalent bond is also consistent with the pyramidalization around the Si atom: The N···SiO and N···SiF angles are 105.6° and 98.4°, respectively. Indeed, the optimized Si···N distance of 1.873 Å is only slightly longer than 1.82 Å, the sum of the C and Si covalent radii. In comparison, the C···N distance of 2.565 Å in Fig. 2e is much longer than the C + N covalent sum of 1.47 Å, albeit quite a bit shorter than the vdW sum of 3.43 Å. The latter comparison comports with the moderate interaction energy of 30 kJ mol^{-1} for F_2CO-IM-TB.

Other parameters listed in Table 1 include first the binding energy E_b which references the dimer energy against that of the two monomers in their fully optimized geometries. The difference between E_b and E_{int} is equal to the deformation energy that the monomers must suffer in order to prepare for the interaction. This difference is quite small, with the exception of the 50 kJ mol^{-1} deformation energy of F_2SiO-IM-TB which is due in part to the pyramidal structure the F_2SiO adopts, mentioned above. The total charge transfer from the Lewis base to the acid, as measured by the sum of natural atomic charges, is contained in Table 1 as CT. This quantity bears a strong relationship to the strength of the bond with the exception of 2IM-π where the two molecules are symmetrically equivalent, and the transfer of charge in one direction from one noncovalent bond is precisely balanced by the transfer in the other direction from the other bond.

The density contour map of NOCV is shown in Fig. S2 (ESI†), in which the electron donor and acceptor are represented in blue and green respectively. A π–π stack has been observed in the 2IM-π system, where the electron density of the C═N π bond of one IM molecule transfers to the empty orbital of the C═N π bond in its partner. In 2IM-HB, the electron density is transferred from the N lone pair of one imidazole into the N–H antibonding orbital of the second imidazole. A similar density contour map of NOCV is seen in F_2CO-IM-HB and F_2SiO-IM-HB. The corresponding NOCV orbital interaction energy (as defined in ref. 42) follows the same pattern as the interaction energy and charge transfer in the three hydrogen-bonded systems. The electron density shifts from the N lone pair electrons in the IM molecule into the C═O antibonding orbital in F_2CO-IM-TB but into the empty orbital of Si in F_2SiO-IM-TB. The NOCV orbital interaction energy is as high as 332 kJ mol^{-1} in the latter complex, further supporting the conclusion that the tetrel bond in this complex is a partially covalent bond.

3.3. Ternary complexes

If a second IM is added to these dimers, one of the ways in which it can position itself is illustrated in Fig. 4a and b for the C and Si systems, respectively. The N of each IM approaches the π-hole above the F_2TO symmetrically from above and below, forming a pair of N···T tetrel bonds. (There is also the possibility of a pair of weaker CH···O HBs, facilitated by the short contact distance despite the unfavorable acute CH···O angles.) As in the dyad cases, the N approaches much closer to Si than to C, 1.997 Å *vs.* 2.731 Å. Because of the negative cooperativity, these distances are both longer than in the TB dyads of Fig. 2.

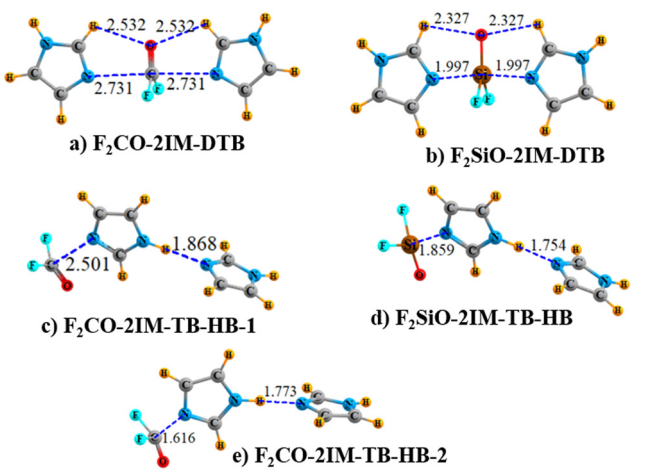

Fig. 4 Optimized geometries of ternary complexes with distances in Å.

Table 4 Total interaction energy (E_{total}) of tetrel bond (E_{TB}), hydrogen bond (E_{HB}), and π–π stacking interaction ($E_{\pi-\pi}$) as well as three-body interaction energy (E_{non}) in the triads. All in kJ mol^{-1}

	E_{total}	E_{TB}	E_{HB}	$E_{\pi-\pi}$	E_{non}
F_2CO-2IM-DTB	−45.65	−26.65	—	—	7.65
F_2SiO-2IM-DTB	−297.27	−167.28	—	—	37.29
F_2CO-2IM-TB-HB-1	−77.78	−30.71	−43.22	—	−3.85
F_2CO-2IM-TB-HB-2	−198.28	−132.13	−41.76	—	−24.39
F_2SiO-2IM-TB-HB	−333.97	−263.63	−42.05	—	−28.29
F_2CO-2IM-HB-TB-π-1	−79.66	−25.69	−12.68	−34.60	−6.69
F_2CO-2IM-HB-TB-π-2	−210.79	−124.64	−3.60	−34.31	−48.24
F_2SiO-2IM-HB-TB-π	−374.51	−259.95	−23.93	−28.33	−62.30

The stretches induced by the presence of the second IM are thus 0.166 and 0.124 Å, as listed in Table S1 (ESI†). Likewise, the total interaction energies of these triads, 45.7 and 297 kJ mol^{-1} for C and Si, respectively, displayed in Table 4, are less than twice the same quantity in the dyads. In fact, the interaction energy of the F_2SiO-2IM-DTB system is only slightly larger than that of F_2SiO-IM-TB.

The energetic manifestation of the negative cooperativity emerges from a computation of the various two and three-body interaction energies. The E_{TB} quantities in Table 4 refer to the interaction energy of the central IM with either of the two F_2TO units, in the absence of the other. The value of −26.65 kJ mol^{-1} listed for the F_2CO-2IM-DTB triad is smaller in magnitude than the −27.55 kJ mol^{-1} reported in Table 1 for the optimized dimer. An even larger margin of −167 and −210 kJ mol^{-1} occurs for the F_2SiO-2IM-DTB. The full interaction energy in each trimer is less negative than twice the 2-body E_{TB}, which is reflected in the positive 3-body nonadditivity term $E_{non} = E_{total} - 2 \times E_{TB}$, in the last column of Table 4.

An alternate arrangement places one of the two IM in the center, flanked by another IM and F_2TO. In this case, the cooperativity ought to be reinforcing as the central molecule acts as an electron donor to the T atom of F_2TO in a TB, and as an electron acceptor in a HB from the other IM. The optimized structures of these arrangements are depicted in Fig. 4c and d. The positive cooperativity reveals itself by the 0.1 Å contraction of the NH···N HB between the two IM units relative to the dimer 2IM-HB. There is also a smaller reduction in the TB lengths. Note also the reinforcing negative values of E_{non} in the last column of Table 4.

It is somewhat surprising to find a second minimum of the F_2CO-IM-TB-HB type. Comparison of Fig. 4e with 4c reveals a 0.8 Å shorter C···N distance within the TB. Indeed this 1.6 Å interatomic distance is barely longer than the 1.47 Å sum of atomic covalent radii. The critical point density of this bond is equal to 0.188 a.u., clearly in the range of covalency, an idea which is seconded by the negative total energy density H of −0.164 a.u. and a large negative density Laplacian of −0.334 a.u. This second minimum type is very close in energy to the first, higher by only 0.85 kJ mol^{-1}. Due to the much closer contacts, the degree of favorable nonadditivity is magnified by a factor of 6, with E_{non} in Table 4 for F_2CO-2IM-TB-HB-2 nearly as large as in the Si analogue. It would seem then that the cooperativity arising from the HB between the two IMs in

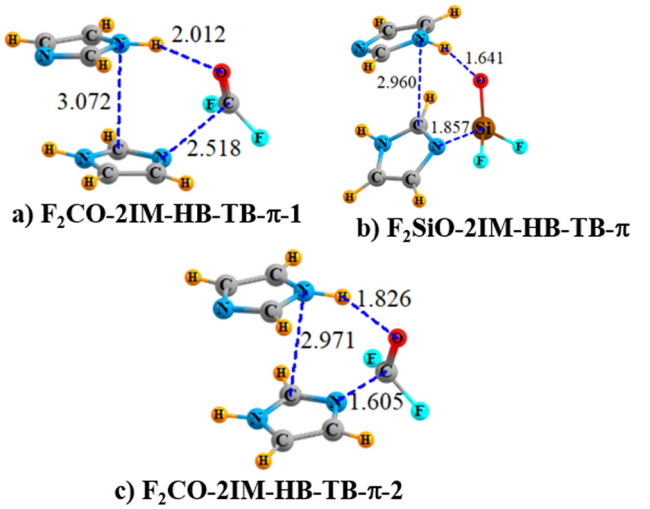

Fig. 5 Optimized geometries of ternary π complexes with distances in Å.

F_2CO-IM-TB-HB-2 facilitates the possibility of a covalent C–N bond, which can compete with the longer noncovalent C···N interaction.

Another mode of building the triad begins with the stacked, slipped parallel IM dimer. Fig. 5 shows how a F_2TO molecule can insert itself in such a way that it forms a TB with the lower IM and a NH···O HB with the upper unit. Once again, the C atom of F_2CO can either lie some distance from the N of IM, 2.518 Å in Fig. 5a, or a second minimum occurs for a closer contact of 1.605 Å in Fig. 5c. The energy of this second minimum is lower in energy than the first by 3.63 kJ mol^{-1}. Whether the first or second type, there is a positive cooperativity as the F_2CO serves as an electron acceptor within the TB and as donor in the HB. There is thus a large negative E_{non} in Table 4, particularly for the second minimum, as well as for the Si analogue. Also, the 2-body terms in Table 4 are all larger in magnitude than the corresponding interaction energies of the dimers in Table 1.

Another measure of the cooperativity is associated with the total charge being transferred from one monomer to the other. This quantity is measured as the total of all of the natural charges in each monomer. In each case, this charge migrates from the unit acting as an electron donor to the acceptor. These transfers are much larger for the TBs than for the HBs as is apparent in Table 5. The effects of cooperativity on these quantities are realized in ΔCT, the difference in the same charge transfer within the triad as compared to the dimer. The negative and positive values of ΔCT comport with the energetics in that positive energetic cooperativity is connected with positive ΔCT, and *vice versa* for negative values. The especially large ΔCT_{TB} for F_2CO-2IM-TB-HB-2 and F_2CO-2IM-HB-TB-π-2 comport with the transition from a weak and long TB in the dimer to a nearly covalent bond in these two triads. Comparison of the AIM diagrams of the dimers in Fig. 3 with those of the various triads in Fig. S3 (ESI†) amplify on the way in which cooperativity is able to strengthen certain bonds. Other manifestations of cooperativity emerge from an examination of

Table 5 Charge transfer within tetrel bond (CT_{TB}) and hydrogen bond (CT_{HB}) in the ternary complexes and their change (ΔCT) relative to the binary analogues, all in e

	CT_{TB}	ΔCT_{TB}	CT_{HB}	ΔCT_{HB}
F_2CO-2IM-DTB	0.006	−0.007	—	—
F_2SiO-2IM-DTB	0.159	−0.045	—	—
F_2CO-2IM-TB-HB-1	0.019	0.006	0.032	0.026
F_2CO-2IM-TB-HB-2	0.470	0.457	0.049	0.019
F_2SiO-2IM-TB-HB	0.217	0.013	0.053	0.024
F_2CO-2IM-HB-TB-π-1	0.013	0	0.004	−0.002
F_2CO-2IM-HB-TB-π-2	0.479	0.466	0.020	0.014
F_2SiO-2IM-HB-TB-π	0.202	−0.002	0.023	0.005

the MEPs of the dimers in comparison to the monomers. For example, formation of the 2IM-HB dimer enhances the negative potential around the N, raising the magnitude of V_{min} from −0.072 to −0.084 a.u., thereby making this IM a more potent nucleophile than is the monomer.

4. Discussion

The stacked IM dimer is strongly reminiscent of the slipped parallel benzene dimer,[47] but its interaction energy of 34.6 kJ mol^{-1} far exceeds that of the latter which is only 10.4 kJ mol^{-1}. One is tempted to attribute this difference in part to the presence of the two heteroatoms in imidazole, and the polarity which they impart to the molecule. Specifically, benzene has no dipole moment so its dimer is incapable of a dipole–dipole stabilization, which is part of the interaction between polar IM units. Not only is the interaction in the imidazole dimer stronger, but also the two molecules move in more closely together. The distance between molecular centers is 3.46 Å, which compares with 4.0 Å in the slipped parallel benzene dimer.

Regarding the tetrel bonds, that between F_2SiO and imidazole is of course very strong, with an interaction energy exceeding 250 kJ mol^{-1}. Although much weaker, the C···N TB in the F_2CO analogue is quite strong on the scale of C-bonds. Its interaction energy of 30 kJ mol^{-1} is itself much larger than that of σ-hole carbon bonds reported in proteins[29] and the π-hole carbon bond in F_2CO complexes with cyanoacetaldehyde[48] and HCN[49] which are less than 20 kJ mol^{-1}. It was noted above that the C···N TB distance of 2.565 Å is quite a bit longer than its Si···N parallel which is only 1.869 Å.

However, there is the possibility of an alternate geometry for the former configuration. In order to probe this issue in more depth, the intermolecular C···N distance in F_2CO-IM-TB was set to a series of values, and for each such distance the remainder of the geometry was fully optimized at the MP2/aug-cc-pVDZ level. In this way, the black curve was traced out in Fig. 6a which indicates a shallow shoulder for a short R(N···C) ∼1.6 Å. Not only is this region shallow, but also its energy is higher than that of the true minimum at R = 2.56 Å by some 15 kJ mol^{-1}. The nature of this curve changes radically, however, when a second IM is added as in the F_2CO-IM-TB-HB triads. As the second IM in Fig. 4 pushes density onto the IM that lies closer to F_2CO, this positive cooperativity makes the N atom on the latter IM a more effective nucleophile, helping it better attract the C. It is this factor that facilitates the appearance of a second minimum, F_2CO-IM-TB-HB-2, with a short R(C···N). The development of this second minimum, not present within the dyad, is clearly evident in the red curve in Fig. 6a. And indeed, this F_2CO-2IM-TB-HB-2 structure is some 5 kJ mol^{-1} more stable than that containing the longer noncovalent bond. There is a barrier separating these two minima, about 5 kJ mol^{-1} higher than the less stable minimum on the right.

This observation raises the question as to whether it is only C for which such a double minimum occurs. Accordingly similar calculations were carried out on the Si and Ge analogs of the F_2CO-IM-TB complex. The black and red curves in Fig. 6b suggest that it is only the short, largely covalent T···N bond that represents a minimum on this surface. There is no hint of a second minimum for a longer separation and a noncovalent bond to either Si or Ge, respectively, quite different in character from the black curve in Fig. 6a with only the barest hint of a shorter C···N minimum in the making.

The short N–C bond in F_2CO-2IM-TB-HB-2 is reminiscent of the tetrahedral intermediate (TI) that might occur if a strong nucleophile like OH^- were to attack the central carbonyl C

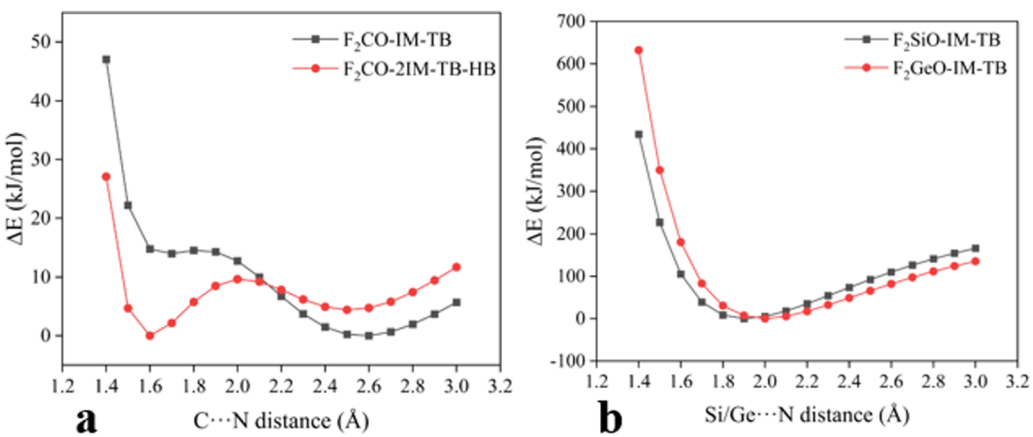

Fig. 6 Relationship between C···N distance and energy in the (a) F_2CO-IM-TB and F_2CO-IM-TB-HB and (b) F_2TO-IM-TB structures at the MP2/aug-ccpVDZ level. Zero energy is taken as the minimum of each.

Table 6 Characteristics of linkage between nucleophile and F_2CO. Charges (q) in e, bond length (r) in Å, angles (θ) in degs, electron density (ρ_{BCP}) in a.u

	F_2CO-2IM-TB-HB-1	F_2CO-2IM-TB-HB-2	F_2CO–$(OH)^-$
r(N/O–C)	2.501	1.616	1.417
r(C═O)	1.182	1.212	1.221
θ(N/O–C–O)	96.3	112.6	118.3
θ(N/O–C–F)	90.5	99.4	103.2
q_O	−0.547	−0.717	−0.776
q_F	−0.319	−0.408	−0.496
q_C	1.158	1.065	1.088
ρ(N/O–C)	0.025	0.189	0.274
ρ(C═O)	0.450	0.430	0.422

atom of the F_2CO. Indeed, such an intermediate lies along the reaction mechanism of the chymotrypsin enzyme, wherein an anionic deprotonated O of a Ser residue attacks the central C of a peptide group.[50–53] This C assumes a tetrahedral coordination, and its C═O group is better approximated as C–O^-. Within the enzyme, this negatively charged oxygen of the tetrahedral intermediate is stabilized by a so-called oxyanion hole filled with H-bonding residues.

This close analogy to such an anionic species is clarified by the data in Table 6 which compares the strongly bound F_2CO-2IM-TB-HB-2 to that in which the pair of IM is replaced by OH^-. The first column of Table 6 includes as a point of reference the F_2CO-2IM-TB-HB-1 structure with the weak and long N···C tetrel bond. The first row explicitly lists the distance from the C of the F_2CO to the nucleophile. The R(NC) distance in F_2CO-2IM-TB-HB-2 is nearly as short as that when the nucleophile is a full-fledged anion. Concomitant with this is the stretch of the internal C═O toward a singly bonded species. The next two rows show that the shorter C···N distance also leads to enlarged angles, and thus to a geometry that more closely approximates the full tetrahedral intermediate with OH^-.

The electronic aspects of these complexes provide further resemblance of F_2CO-2IM-TB-HB-2 to the TI with OH^-. One can see that the natural charge of the carbonyl O becomes much more negative as the nucleophile approaches more closely, and the C═O mutates toward C–O^-; a similar increased negative charge occurs for the two F atoms. Note also that the central C atom becomes less positive, a sign of the extra density that is being acquired from the nucleophile. The last two rows of Table 6 report the densities of the indicated bond critical points. That between the nucleophile and the central C is of course much larger for the closer approach. And the transition from a double C═O to a single C–O bond is consistent with the reduced density in the final row.

Note that in all cases, the parameters of the F_2CO-2IM-TB-HB-2 complex are fairly close to that of F_2CO-$(OH)^-$, which is impressive in light of the absence of a negative charge on the nucleophile in the former case. Indeed, it is an important finding here that the pair of IM units, along with the HB between them, can induce bonding and other changes in the F_2CO that are nearly as large in magnitude as that caused by a powerful anionic nucleophile like OH^-. It should be added parenthetically that a similarly short intermolecular bond, along with the partial transition to a TI occurs for F_2SiO, even when the nucleophile is a single IM, with no need for the cooperativity of the IM dimer.

It should be added finally that there is precedent for the idea that both a close and distant encounter complex can coexist. Grabowski's calculations[54] had observed a parallel occurrence in the B···N triel bond when BX_3 (X = Cl, Br, I) is paired with NCH. It is hoped that these earlier results, coupled with the findings reported here, may stimulate further inquiries, of both computational and experimental natures, into this sort of bond stretch isomerism.

5. Conclusions

A pair of imidazole units can complex with one another so as to form either a NH···N HB or a slipped parallel geometry. Both are fairly strong interactions, with the former somewhat lower in energy. IM can engage in a NH···O HB with the O atom of F_2TO, which is quite a bit stronger for T = Si than for C. The strongest binding between IM and F_2TO arises when the N of IM approaches the π-hole that lies above the T atom. This tetrel bond is twice as strong as the HB for C. In the case of F_2SiO, the IM approaches much more closely to the Si forming a much shorter and stronger covalent bond, with an interaction energy exceeding 250 kJ mol^{-1}.

There are several geometric configurations possible when a second IM is added to the IM/F_2TO pair. Each IM can approach from above and below the T atom to form two TBs to this same atom. The negative cooperativity arising from the central T acting as an electron acceptor in two separate TBs reduces the interaction energy well below twice the single TB energy within the IM/F_2TO dimer. An alternate configuration which takes advantage of positive cooperativity places the second IM in a location where it can form a HB through the NH group of the first IM. The total interaction energies here are larger than the simple sum of the individual energies within the dimers, and intermolecular distances reduced. An alternate structure places the F_2TO near the slipped parallel stacked IM dimer, in a position where it can engage in a NH···O HB with one IM and a T···N TB with the other. The presence of three intermolecular bonds, in concert with positive cooperativity, makes these trimers the most stable of all.

One of the most fascinating aspects of these complexes arises in the context of F_2CO. Unlike the covalent T–N bond formed with IM by F_2SiO (or F_2GeO for that matter), that with F_2CO remains much longer and clearly noncovalent. However, when the electron donating ability of IM is enhanced by its interaction with a second IM, a much shorter covalent C–N bond becomes a real possibility. Both the latter covalent bond, and the longer C···N noncovalent bond, represent minima on the potential energy surface, with a barrier of some 5 kJ mol^{-1} separating them. But it is the shorter covalent bond that is energetically preferred. This same sort of dual covalent/noncovalent possibility occurs also when the F_2CO approaches the two IM units arranged in their stacked geometry.

Author contributions

XW: carried out calculations and helped write manuscript; QL: formulated project and contributed to manuscript; SS: guided project and wrote final manuscript.

Conflicts of interest

The authors declare no conflicts of interest.

Acknowledgements

This work was supported by the Natural Science Foundation of Shandong Province (ZR2021MB123) and the US National Science Foundation (1954310)

References

1 A. Langner, S. L. Tait, N. Lin, C. Rajadurai, M. Ruben and K. Kern, *Proc. Natl. Acad. Sci. U. S. A.*, 2007, **104**, 17927–17930.
2 R. Raucci, E. Laine and A. Carbone, *Structure*, 2018, **26**, 905–915.
3 G. Tárkányi, P. Király, S. Varga, B. Vakulya and T. Soós, *Chem. – Eur. J.*, 2008, **14**, 6078–6086.
4 G. C. Pimentel and A. L. McClellan, *Annu. Rev. Phys. Chem.*, 1971, **22**, 347–385.
5 W. Lu, M. C. Chan, N. Zhu, C. M. Che, Z. He and K. Y. Wong, *Chem. – Eur. J.*, 2003, **9**, 6155–6166.
6 K. E. Riley, M. Pitoňák, P. Jurečka and P. Hobza, *Chem. Rev.*, 2010, **110**, 5023–5063.
7 K. Muller-Dethlefs and P. Hobza., *Chem. Rev.*, 2000, **100**, 143–168.
8 S. Scheiner, *Noncovalent Forces*, Springer, 2015, pp. 47–68.
9 P. Hobza, R. Zahradnik and K. Muller-Dethlefs, *Collect. Czech. Chem. Commun.*, 2006, **71**, 443–531.
10 S. Scheiner, *Hydrogen bonding: a theoretical perspective*, Oxford University Press, 1997.
11 G. A. Jeffrey, *An introduction to hydrogen bonding*, Oxford university press, New York, 1997, vol. 12, p. 228.
12 M. Hennemann, J. S. Murray, P. Politzer, K. E. Riley and T. Clark, *J. Mol. Model.*, 2012, **18**, 2461–2469.
13 P. Politzer, J. S. Murray and T. Clark, *Phys. Chem. Chem. Phys.*, 2013, **15**, 11178–11189.
14 P. Metrangolo, F. Meyer, T. Pilati, D. M. Proserpio and G. Resnati, *Chem. – Eur. J.*, 2007, **13**, 5765–5772.
15 S. Scheiner, *Chem. Phys. Lett.*, 2011, **514**, 32–35.
16 S. J. Grabowski, *Chem. – Eur. J.*, 2013, **19**, 14600–14611.
17 R. S. Ruoff, T. Emilsson, A. I. Jaman, T. C. Germann and H. S. Gutowsky, *J. Chem. Phys.*, 1992, **96**, 3441–3446.
18 K. Tamao, T. Hayashi and Y. Ito, *J. Organomet. Chem.*, 1996, **506**, 85–91.
19 R. D. Urban, G. Rouillé and M. Takami, *J. Mol. Struct.*, 1997, **413**, 511–519.
20 N. W. Mitzel, A. J. Blake and D. W. H. Rankin, *J. Am. Chem. Soc.*, 1997, **119**, 4143–4148.
21 N. W. Mitzel and U. Losehand, *Angew. Chem., Int. Ed.*, 1997, **36**, 2807–2808.
22 K. B. Borisenko, R. O. Gould, C. A. Morrison, S. Parsons and D. W. H. Rankin, *J. Mol. Struct.*, 2000, **554**, 163–172.
23 I. Alkorta, I. Rozas and J. Elguero, *J. Phys. Chem. A*, 2001, **105**, 743–749.
24 S. Scheiner, *Phys. Chem. Chem. Phys.*, 2021, **23**, 5702–5717.
25 T. Clark, M. Hennemann, J. S. Murray and P. Politzer, *J. Mol. Model.*, 2007, **13**, 291–296.
26 S. J. Grabowski, *Phys. Chem. Chem. Phys.*, 2014, **16**, 1824–1834.
27 D. Mani and E. Arunan, *Phys. Chem. Chem. Phys.*, 2013, **15**, 14377–14383.
28 X. García-LLinás, A. Bauzá, S. K. Seth and A. Frontera, *J. Phys. Chem. A*, 2017, **121**, 5371–5376.
29 V. R. Mundlapati, D. K. Sahoo, S. Bhaumik, S. Jena, A. Chandrakar and H. S. Biswal, *Angew. Chem., Int. Ed.*, 2018, **57**, 16496–16500.
30 M. Hou, Z. Liu and Q. Li, *Int. J. Quantum Chem.*, 2020, **120**, e26251.
31 S. Chandra, N. Mahapatra, N. Ramanathan and K. Sundararajan, *Chem. Phys. Lett.*, 2023, **828**, 140722.
32 Z. Rezaei, M. Solimannejad and M. D. Esrafili, *Comput. Theor. Chem.*, 2015, **1074**, 101–106.
33 S. Scheiner, *Chem. – Eur. J.*, 2016, **22**, 18850–18858.
34 S. Scheiner, *J. Phys. Chem. A*, 2021, **125**, 2631–2641.
35 M. J. Frisch, G. W. Trucks, H. B. Schlegel, G. E. Scuseria, M. A. Robb, J. R. Cheeseman, G. Scalmani, V. Barone, B. Mennucci, G. A. Petersson, H. Nakatsuji, M. Caricato, X. Li, H. P. Hratchian, A. F. Izmaylov, J. Bloino, G. Zheng, J. L. Sonnenberg, M. Hada, M. Ehara, K. Toyota, R. Fukuda, J. Hasegawa, M. Ishida, T. Nakajima, Y. Honda, O. Kitao, H. Nakai, T. Vreven, J. J. A. Montgomery, J. E. Peralta, F. Ogliaro, M. Bearpark, J. J. Heyd, E. Brothers, K. N. Kudin, V. N. Staroverov, R. Kobayashi, J. Normand, K. Raghavachari, A. Rendell, J. C. Burant, S. S. Iyengar, J. Tomasi, M. Cossi, N. Rega, J. M. Millam, M. Klene, J. E. Knox, J. B. Cross, V. Bakken, C. Adamo, J. Jaramillo, R. Gomperts, R. E. Stratmann, O. A. Yazyev, J. Austin, R. Cammi, C. Pomelli, J. W. Ochterski, R. L. Martin, K. Morokuma, V. G. Zakrzewski, G. A. Voth, P. Salvador, J. J. Dannenberg, S. A. Dapprich, D. Daniels, O. Farkas, J. B. Foresman, J. V. Ortiz, J. Cioslowski and D. J. Fox, *Gaussian 09, Revision A.02*, Gaussian, Inc., Wallingford, CT, 2009.
36 S. F. Boys and F. Bernardi, *Mol. Phys.*, 1970, **19**, 553–556.
37 F. Biegler-Konig, AIM2000, University of Applied Sciences, Bielefeld, Germany, 2000.
38 T. Lu and F. Chen, *J. Comput. Chem.*, 2012, **33**, 580–592.
39 W. F. Humphrey, A. Dalke and K. Schulten, *J. Mol. Graphics*, 1996, **14**, 33–38.
40 A. Otero-De-La-Roza, E. R. Johnson and J. Contreras-García, *Phys. Chem. Chem. Phys.*, 2012, **14**, 12165–12172.
41 A. E. Reed, L. A. Curtiss and F. Weinhold, *Chem. Rev.*, 1988, **88**, 899–926.
42 M. P. Mitoraj, A. Michalak and T. Ziegler, *J. Chem. Theory Comput.*, 2009, **5**, 962–975.

43 A. A. Granovsky, M. W. Schmidt, K. K. Baldridge, J. A. Boatz and K. A. Nguyen, *J. Comput. Chem.*, 1993, **14**, 1347–1363.
44 P. Su and H. Li, *J. Chem. Phys.*, 2009, **131**, 014102.
45 Q. Tang and Q. Li, *Comput. Theor. Chem.*, 2014, **1050**, 51–57.
46 A. P. L. Rendell, G. B. Bacskay and N. S. Hush, *Chem. Phys. Lett.*, 1985, **117**, 400–408.
47 S. Tsuzuki, K. Honda, T. Uchimaru, M. Mikami and K. Tanabe, *J. Am. Chem. Soc.*, 2002, **124**, 104–112.
48 Y. Wei and Q. Li, *Mol. Phys.*, 2018, **116**, 222–230.
49 M. Vatanparast, E. Parvini and A. Bahadori, *Mol. Phys.*, 2016, **114**, 1478–1484.
50 J. J. Birktoft and D. M. Blow, *J. Mol. Biol.*, 1972, **68**, 187–240.
51 G. Robillard and R. G. Shulman, *J. Mol. Biol.*, 1927, **71**, 507–511.
52 S. Scheiner, D. A. Kleier and W. N. Lipscomb, *Proc. Natl. Acad. Sci. U. S. A.*, 1975, **72**, 2606–2610.
53 S. Scheiner and W. N. Lipscomb, *Proc. Natl. Acad. Sci. U. S. A.*, 1976, **73**, 432–436.
54 S. J. Grabowski, *J. Comput. Chem.*, 2018, **39**, 472–480.

